Lawrence Berkeley Laboratory
UNIVERSITY OF CALIFORNIA, BERKELEY, CA

Materials & Molecular
Research Division

THE EFFECT OF AIR-COOLING HEAT TREATMENTS ON THE STRUCTURE AND PROPERTIES OF Fe/4Cr/0.3C/2Mn ALLOY

Thomas Hugh Rabe
(M. S. thesis)

June 1979

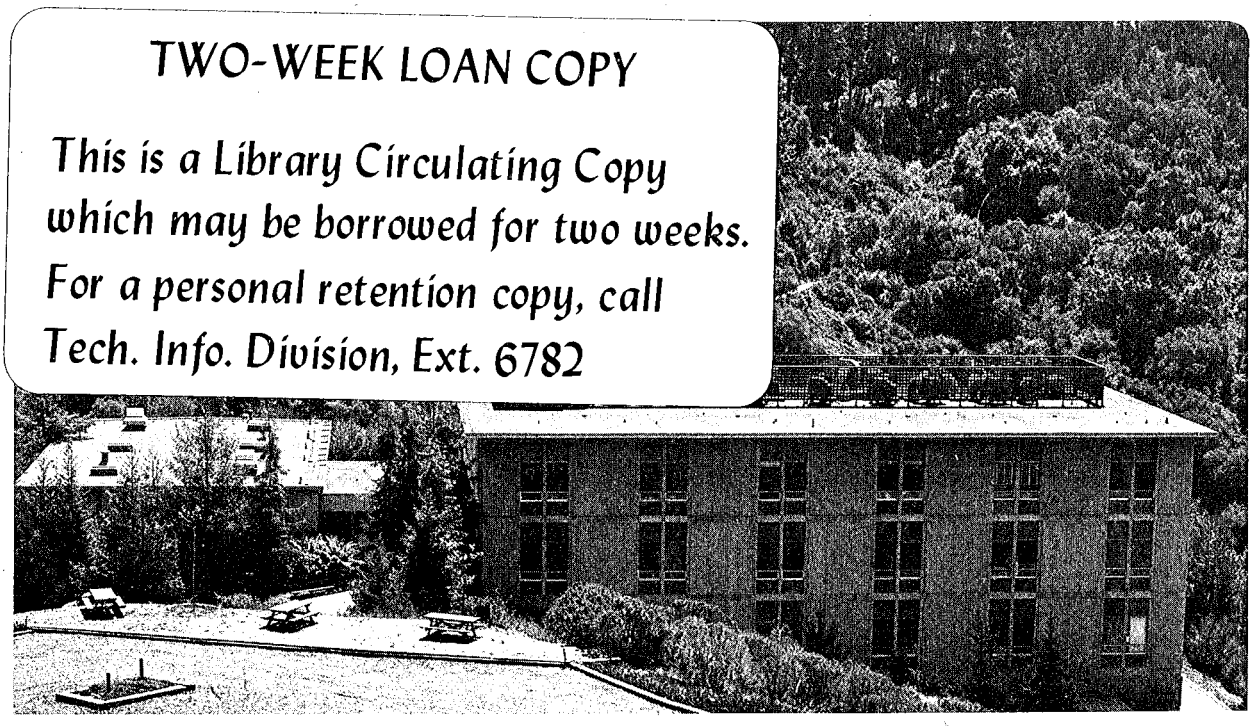

Prepared for the U. S. Department of Energy
under Contract W-7405-ENG-48

I. INTRODUCTION

It is well known that the martensitic transformation can be exploited to produce a wide variety of strength-toughness combinations in structural steels. However, a complete and self consistent understanding of these effects is not available.[1,3] In order to amend this situation, a program of systematic investigations of the influence of alloying and heat treatment on martensite microstructures and resultant mechanical properties has been in progress at Berkeley for the past several years.[4-10] The foundation of this research is the use of simple, high purity alloys which allows the study of isolated effects of individual alloying additions by minimizing the mutual interaction effects of multiple alloying agents. The ternary Fe/Cr/C alloy system has been used as a base for quarternary and quinternary alloy additions, largely because this system is well documented and is known to have excellent combinations of properties as compared to other commercial alloys.[4,7,11,12]

An important observation to come out of this work[4,13] is the identification of thin interlath films of retained austenite in alloys at temperatures well below their apparent M_f temperatures. Since this discovery, which employed high resolution electron microscopy, many investigators have attributed improved toughness to these films.[4,8-10,14-16] Indeed, the chemical thermal and mechanical stabilization of austenite, along with its morphology, may have a profound effect on toughness in many alloys. It is therefore an integral part of these investigations to assess unambiguously the role of retained

austenite in providing toughness in steels, by varying alloy additions and heat treatments.

One of the most promising alloys to emerge from this research is Fe/4Cr/0.3C/2Mn. As shown by Rao,[9,10] when properly heat treated, this alloy has a combination of strength and toughness properties superior to most commercially available alloys. Although encouraging, these results rely on various quench and temper heat treatment. It is the purpose of this investigation to study the feasibility of simple heat treatments involving air-cooling from the austenitic phase region. This work is of interest for several reasons. If it is possible to produce reasonable mechanical properties in this alloy using simple heat treatments, the cost and amount of energy necessary to produce the alloy will be reduced. Also, by understanding air-cooling behavior, we gain some insight into the weldability of the alloy as well as its usefulness when produced for thick-section applications.[15]

The single, and yet crucial variable in air-cooling, is the austenitization temperature. Undissolved carbides can reduce an alloy's resistance to fracture[17,18] by providing an easy crack path if the interfacial cohesion is poor. It has also been shown, that during ductile fracture the resistance to fracture decreases with increasing inclusion size.[19] The austenitization temperature directly controls the degree to which carbides and other inclusions are taken into solution. It has been shown by Rao[20,30] that one hour at 1100 ^{o}C is sufficient to dissolve most carbides. However lower temperature treatments are economically more favorable. Therefore we have chosen to austenitize

at 1050°C as well as 1100°C. Also, in order to modify segregation effects by tying up segregating species in pre-existing inclusions,[31] a still lower austenitization temperature of 900°C is used. At lower temperatures, austenite grain growth is also reduced, which may be extremely important in this manganese modified alloy, since it has a tendency for grain growth.[9] Reduced grain size is found to lower the Ductile Brittle Transition Temperature[21,22] as well as decrease the severity of segregation of embrittling constituents.[23] These treatments have all been studied with and without subsequent tempering treatments at 200°C.

II. EXPERIMENTAL PROCEDURE

A. Materials Preparation

The material used for tensile, and initial Charpy-V-Notch impact toughness specimens were supplied by Daido Steel Company in Japan in the form of 1/2 in. dia. rods and 2.5 in. wide by 1 in. thick bars. Further Charpy-V-Notch impact toughness specimens and K_{IC} plane strain fracture toughness specimens were cut from material produced at Lawrence Berkeley Labs. This material was supplied in the form of round ingots, which were subsequently rolled into 2.5 in. wide by 1 in. thick bars. The chemical compositions of this vacuum melted alloy (after homogenization at 1200°C for 24 hrs and furnace cooled) is given in Table I.

B. Heat Treatment

All austenitizing treatments were carried out in vertical tube furnaces under argon atmosphere. Oversized tensile, Charpy and K_{IC} specimens were cut from their respective stock, with final machining being done under flood cooling after heat-treatment. Tempering treatments were performed by immersing the specimens for one hour in an alumina bed fluidized with argon and maintained at the required temperature. At the end of tempering treatments, all specimens were water quenched. The air-cooling treatment is illustrated in Fig. 1. This cooling curve was produced by inserting a thermocouple into a hole drilled in a K_{IC} specimen blank and monitoring the temperature for one hour after the specimen was removed from the furnace.

C. Dilatometry

A commercial dilatometer (Theta Dilatronic III R dilatometer) was used to establish the phase transformation temperatures, viz., M_s, M_f, austenite start temperature, A_s, and austenite finish temperature, A_f, of the alloy.

D. Mechanical Testing

1. Tensile Testing

The dimensions of the 1.25 in. gauge length, round tensile specimen are shown in Fig. 2(A). Tensile testing was done at room temperature in a 300 Kip capacity MTS testing machine at a cross head speed of 0.04 in./min.

2. Fracture Toughness Testing

Plane strain fracture toughness values were obtained by testing standard compact tension, crack-line loaded toughness specimens shown in Fig. 2(B). Following heat-treatment, at least 0.01 in. was removed from both sides of the K_{IC} blanks. The thickness for all of the specimens conformed to the ASTM specifiications[24] for the plane strain condition. The 300 Kip MTS machine was used for fatigue precracking the specimens to a minimum crack length of 0.05 in., which were subsequently tested in the same machine to obtain the fracture toughness data. The orientation of crack propagation with respect to the long dimension of the bar stock is L-T.[24]

3. Charpy Impact Testing

Standard Charpy-V-Notch specimens shown in Fig. 2(C) were obtained from oversized heat-treated blanks. A minimum of 2, and in the 900°C

case, 5 Charpy-V-Notch specimens were tested and the tabulated results correspond to the average of these tests.

E. Metallography

1. Optical Metallography

Specimens for optical metallography were cut from broken Charpy bars, mounted in koldmount, abraded on silicon carbide papers down to 600 grit, polished on a 1 μm diamond abrasive wheel and finally polished with 0.3 μm alumina in a vibrating polishing machine. Microstructures were revealed by etching specimens in 2% and 5% nital solutions and in a 5% picral solution.

2. Electron Metallography

Thin foils for transmission electron microscopy were obtained from heat-treated and fractured K_{IC} test specimens. About 20 mil thick slices were cut from these specimens, and following cleaning to remove any oxide scale, these were chemically thinned to less than 5 mils at room temperature in a solution of 4-5% HF in H_2O_2. Following chemical thinning 3.00 mm disks were spark cut from these slices and hand ground down to less than 2 mils thick. These discs were finally electropolished in a twin jet electro-polishing apparatus at room temperature, using a chromic-acetic acid solution of 75 gm CrO_3, 400 ml CH_3COOH and 21 ml distilled water. The polishing voltage varied from 35-50 volts. Thin foils so obtained, were stored in alcohol and subsequently examined in JEM 7A and Philips EM 301 microscopes at an operating voltage of 100 kV.

3. Scanning Electron Microscopy and Energy Dispersive Analysis of X-rays

Fractography was conducted on both K_{IC} and Charpy specimens, using an AMR-1000 scanning electron microscope at 20 kV. The fracture surfaces were preserved by masking with tape during cutting and preparation of the specimen. This tape was later dissolved in acetone. An X-ray energy dispersive analysis (EDAX) unit, attached to the microscope allowed the semi-quantitative analysis of inclusions and precipitates to be carried out.

F. X-ray Analysis

X-ray analysis was used to monitor the volume percent of retained austenite after the 900°C and 1100°C austenitization and air-cooled heat treatments. For this purpose broken Charpy specimens were used. After repeated mechanical polishing and etching in a solution containing 100 ml H_2O_2 and 4 ml HF to obtain a shiny surface, the specimens were scanned in a Picker X-ray diffractometer with a fixed horizontal stage using CuKα radiation. The scan angle (2θ) covered was from 40° to 100° which includes the prominent $(111)_\gamma$, $(311)_\gamma$, $(220)_\gamma$, and $(222)_\gamma$ reflections. Tests were performed at room temperature in both the as-cooled and cooled and quenched in liquid nitrogen conditions.

III. RESULTS

A. Air-Cooling Time vs. Temperature Curves

Cooling curves for the 900°C and 1100°C heat treatments have been experimentally produced (Fig. 1). As can be seen, both treatments allow rapid cooling to about 500°C. Below this temperature however, cooling begins to slow. As is demonstrated, both treatments allow the alloy to spend significant amounts of time above its M_s temperature. As is expected, the actual time above M_s (15 minutes for 1100°C) is dependent on the "heat content" of the specimen, which in turn depends on the original austenitization temperature.

Also shown in Fig. 1, is the bainitic start and 95% completion curves from a Fe/4Cr/0.4C steel TTT diagram produced elsewhere.[12] These lines are not intended to represent the steel under observation, but are included for reference. Since the alloy of this investigation contains 2 w/o Mn, which is known to suppress both the martensitic[27] and bainitic transformations, the actual bainite transformation curves are likely to be displaced down and to the right, from those presented.

B. Mechanical Properties

The mechanical properties of the alloy in the as-cooled and as-cooled temper conditions are summarized in Table III.

1. Tensile Properties

Rao[9] has shown that as-quenched yield and ultimate tensile strengths for this alloy are 207 KSI and 265 KSI respectively. Tempering at 200°C is found to decrease these values to 195 KSI and 235 KSI respectively. These strengths correspond roughly with those found here. This is reasonable, in that auto-tempering occurs during the slow cooling.

The slight reduction in yield strength at lower austenitization temperatures is most probably the result of lower carbon content in the matrix due to the presence of undissolved carbides.[30]

2. Fracture Properties

Both plane strain fracture and Charpy impact toughness tests show poor fracture properties in all cases tested. Rao[9,10] has achieved a calculated K_{IC} toughness of 180 KSI-in.$^{1/2}$ from K_Q values, and Charpy impact toughness of 40 ft-lbs. It is found the decreased austenitization temperature increases Charpy impact toughness to some degree, while K_{IC} values remain essentially constant. This may be a consequence of the variation in grain size, which is known to strongly affect impact toughnesses.[21,22]

C. Microstructural Characterization

1. Optical Metallography

Optical metallography was employed to measure prior austenite grain sizes and detect any gross variations in microstructure, such as coarse undissolved carbides. Figure 3 shows a representative optical micrograph for each treatment performed, and the variation in prior austenite grain size is recorded in Table II. Due to the complex, fine microstructure, observations by optical means are difficult and no major differences could be easily noted, with the exception of packet and grain size variations as noted in Table II.

2. Transmission Electron Microscopy

Structural characterization by transmission electron microscopy was limited to 1100°C and 900°C as-cooled heat treatments, in order to isolate the effect of air-cooling in the extreme cases of treatment.

Of these two treatments, the 1100°C case received the most concentrated investigation, since it represents the most severely degraded toughness properties.

Parallel lath morphologies are evident in all foils examined (Figs. 5, 6, 8 and 9). The special case of laths being viewed edge on and in lateral section, is shown in Fig. 9. In the majority of cases, this lath morphology can be conclusively identified as that of dislocated martensite (Figs. 6 and 9) or possibly lower bainite with its typical internal carbides.[12,26] It is also found that relatively little substructural twinning occurs in this alloy (Fig. 5), as is expected due to the carbon content.[4,26] Another important observation is that a large volume fraction of retained austenite exists after air-cooling. As has been accomplished by other investigators using careful electron microscopy techniques,[4,8,13] retained austenite has been imaged in DF using the $(200)_\gamma$ reflection as described elsewhere[8,13] (Figs. 6(b) and 8(b)). It has been observed that retained austenite exists as thin, semi-continuous, interlath films (Fig. 6(b)), and that the amount and morphology of retained austenite does not significantly vary with austenitization temperature. Well established $\langle 110 \rangle_\alpha$ widmanstatten cementite platelets are found within the martensitic laths, indicative of extensive auto-tempering (Fig. 7 and 10). These carbides are very similar in nature to those found after quench and temper heat treatments.[9,10] These cementite platelets are about 300A wide and 0.3 μm long.

In addition to lath martensite, a different microstructural constituent exists in Fig. 8. This is the charcteristic microstructure of lower bainite. As has been observed before,[12,26] carbides are oriented

at 50-60° angles to the long direction of laths. This orientation is maintained in several adjacent laths. As can also be seen in Fig. 8(b), carbide layers are found to occur at bainite lath boundaries. From the examination of several foils, the volume fraction of bainite in the 1100°C case is estimated to be about 10%, while in the 900°C case it represents less than 5% of the observed structure.

Another feature of these microstructures, is the existence of large numbers of undissolved carbides, as shown in Fig. 5. Although sometimes quite large (diameters greater than 1 μm), these carbides average about 0.2 μm in diameter in the 1100°C treatment and 0.6 μm in diameter in the 900°C treatment. The lowered austenitization temperature favors the retention of these carbides, and a larger number are observed in this case. Since the foils used for transmission electron microscopy come from broken K_{IC} specimens, these carbides are assumed to be the same as those in K_{IC} fracture surfaces, which are found to be titanium based, as discussed in the next section.

3. X-ray Volume Fraction Analysis

Measurements of the volume fraction of retained austenite in the as-cooled 900°C and 1100°C austenitization treatments were performed using x-ray analysis. In order to study the stability of the retained austenite, these measurements were repeated after the samples had been quenched in liquid nitrogen. The results of these procedures are summarized in Table IV. The volume fractions in the as-cooled conditions, agree well with estimates made using transmission electron microscopoy. It is also found that cooling the specimens to liquid nitrogen temperatures (77°K) does not markedly change the

retained austenite volume fraction in the 1100°C case, but shows significant reduction in the 900°C treatment.

D. Fractography and Particle Characterization

Fractography was performed on the fracture surfaces of both Charpy and K_{IC} toughness specimens. Figure 11(c) and (d) shows clearly that for the 1100°C treatment, brittle quasi-cleavage fracture occurs in the Charpy tests. An interesting feature of these fractographs is the parallel ridges which occur on the fracture surface. These indicate severe interlath tearing or fracture. The separation of these ridges is roughly equivalent to the average lath widths in Table II. In the 900°C impact toughness fractographs (Fig. 11(a) and (b)), fracture occurs by a mixed mode of ductile dimpled rupture and brittle, quasi-cleavage fracture. Evidence of parallel ridges can be seen in the cleavage regions, and most dimples are associated with spherical inclusions (Fig. 12).

The fractographs from K_{IC} toughness tests (Fig. 13) all show a similar mixed mode of fracture, with dimpled rupture appearing to be the predominant mode. Parallel ridge structures again appear in some areas, but they are much less obvious than in the Charpy surfaces. A large number of spherical precipitates associated with dimples, are easily observable in these fracture surfaces.

An x-ray energy dispersive analysis (EDAX) unit attached to the scanning electron microscope was used to qualitatively characterize the inclusions found in these fracture surfaces. Figs. 12 and 14 show such characterizations for Charpy and K_{IC} tests, respectively. For 900°C austenitization, particles are found to average about 3 μm

in diameter and for 1100°C austenitization they are less than 1 μm in diameter on the average. By comparison to average diameters observed in TEM, these results indicate that the larger undissolved particles are involved in fracture. In Charpy fracture surfaces (Fig. 12(a) and (b)), inclusions can be identified as (Mn, Fe) S particles (Fig. 12(c) and (d)). In the K_{IC} fracture surfaces (Fig 14(a) and (b)), particles observed are for the most part characterized as titanium based carbides or perhaps titanium and aluminum oxides. These differences are explained by the fact that the material used to make specimens for the Charpy and K_{IC} tests came from different sources.

IV. DISCUSSION

In this steel, the air-cooling heat treatment produces large volume fractions of dislocated lath martensite (Figs. 5, 6 and 9), which have morphologies quite similar to those produced through quench and temper heat treatments.[9] This is a reasonable result in that the high hardenability of this steel (calculated critical diameter greater than 12 inches) due to its total alloy content (C, Mn and Cr), should guarantee nearly 100% martensite in thick specimens.[32] The existence of widmanstatten cementite platelets is also understandable in that during slow cooling below the M_s temperature, sufficient time is allowed to form carbide precipitates as a result of autotempering. This martensite morpohology along with the existence of fine interlath films of retained austenite, as illustrated in Fig. 4, have been shown to have excellent strength and toughness properties,[9] and these austenite films are indeed observed in air-cooled specimens (Fig. 6(b)). The stabilization of austenite, as observed here and in evidence in Table IV, may be the result of the combined influence of chemical[28] and thermal[29] stabilization, which are enhanced by slow cooling, and mechanical stabilization,[11] which should be decreased due to the increased ability of carbon to migrate away from the austenite/martensite interface. Since austenite films appear fequently and as fairly continuous layers, it is expected that this martensite/anstenite structure is strong and tough. Therefore the low toughnesses encountered must be due to other microstructural features.

The existence of large undissolved carbides most certainly plays an important role in degrading toughness properties. As Rao[9] points

out, these particles are remnants of prior treatments and in most cases will be incoherent with the austenite matrix, causing carbide/matrix interface cracking or the build up of residual stresses at these interfaces during the austenite to martensite shear transformation. Hence fast, brittle fracture will be favored and the steel's toughness will be reduced. At the same time however, these inclusions tie up deleterious segregating species and may reduce the occurrence of embrittlement due to segregation. This may in part explain the change in the impact toughness fracture mode from the 900°C austenitization treatment (Fig. 11(a) and (b)) where inclusions are intimately involved in the fracture mechanism, to the 1100°C austenitization treatment (Fig. 11(c) and (d)) where inclusions are not as obviously involved in fracture. These results indicate that although the presence of large undissolved carbides degrades toughness properties, dissolution of these inclusions, and the resultant increase in segregation effects, may cause even greater embrittlement problems.

Figure 8 demonstrates the existence of lower bainite in the 1100°C heat treated specimens. The time spent above the M_s temperature must therefore be long enough to cross the B_s transformation curve for this alloy. This is found to be true for both heat treatments. Pickering[25] points out that the degree to which the bainitic transformation curve is suppressed downward by alloying elements directly reflects the tendency toward transformation to a lower bainitic structure. This, along with the fact that cooling curves (Fig. 1) indicate that an appreciable amount of time is spent just above the M_s temperature, provide adequate explanation of the lower bainitic structure observed.

But there is also interference from the upper bainitic reaction occurring. This is indicated by nearly continous films of carbide as shown in the dark field micrograph, Fig. 8(b). While lower bainite structures can be quite strong and tough, the interference of upper bainite has been found to produce low toughnesses by other investigators,[6,7,12] especially when compared to the high toughness of dislocated martensite. Altough the reasons for this behavior are not clearly understood, it may in part explain the low toughnesses measured here. The spacings between parallel ridges observed in Fig. 11(d) correspond roughly to the width of bainite laths and indicate fracture along bainite plate boundaries. Very similar fracture surfaces have been observed in nearly 100% bainitic steels.[12] These indicate that the incoherency of the carbid/ferrite interface and segregation of impurities at those interfaces, play important roles in degrading toughness. The observed change in fracture mode and slight change in toughness in the Charpy tests (Fig. 11 and Table III) can now be understood. In the 1100°C austenitization, the larger volume fraction of bainite due to the longer times above the M_s temperature and more pronounced segregation effects therein, embrittle the material. In the 900°C austenitization, both of these factors are reduced, but increased undissolved carbides causes low toughness. This does not adequately explain the plain strain fracture behavior which always seems to involve inclusions; although this latter case may be result of the large number of impurity carbides, etc. in the material, and indeed may not be a fair test of the plane strain fracture toughness this alloy can possess when air cooled.

It is clear that the loss of toughness in this alloy on air cooling has not been explained adequately. The overlapping effects of decomposition products and undissolved carbides make the investigation difficult. Further work must be done to resolve the exact mechanism which causes this embrittlement. In particular, heat treatments which preclude the possibility of producing bainite (hot water quench or forced air cooling) must be investigated. Also the nature of ferrite/carbide interfaces in bainite must be studied to explain the low toughnesses which have been observed here and in other cases, when upper bainite is present. In total, this work suggests the study of this alloy austenitized at a high temperature (1100^{o}-1150^{o}C) to dissolve carbide structures entirely and then quickly cooled (hot water quench) to temperatures below the M_s temperature. It must also be recognized, that this work also indicates the use of this alloy in thick sections, or in welded applications may be limited due to the slow cooling rates these uses may involve.

V. CONCLUSIONS

Based on the present study of the air cooling of the high strength, high toughness alloy Fe/4Cr/0.3C/2M_n, the following conclusions can be drawn:

1. It has been shown that although the strength of the alloy is only mildly affected by air-cooling, fracture toughness properties are severely degraded.

2. A disslocated lath martensite and retained austenite film morphology has been identified as the predominent microstructure after air cooling. Since this structure has been shown to exhibit high strength and toughness, it is suggested that this feature of the microstructure has little to do with the low toughness values found here.

3. The austenite decomposition products of both upper and lower bainite hve been identified, with a total volume fraction of less than 10%. It is supposed that either the interference of upper bainite or large undissolved carbides cause reduced toughnesses in the heat treatments tested.

4. Favorable strength and toughness properties may be obtainable with this alloy by using austenitization temperatures high enough to insure the dissolution of carbides (1100^{o}C) and somewhat faster cooling rates, such as those produced by hot water quenching or forced air cooling.

ACKNOWLEDGMENTS

As is most often the case, an investigation of this nature is the combined effort of many individuals. With gratitude to all of these people, the author wishes to especially thank Professor Gareth Thomas and Dr. B. V. Narasimha Rao for their enthusiastic guidance and unfailing support throughout this work. He also wishes to thank Professors I. Finnie and J. W. Morris Jr. for their critical review of this manuscript.

The able assistance of the support staff of the Materials and Molecular Research Division of the Lawrence Berkeley Laboratory is also gratefully acknowledged. In particular, the technical skills, patience, friendship and ability with a crossword of Carolyn Gosnell are recognized.

Finally, the author is indebted to Elizabeth Wolcott Aldrich who provided all the things no one else could, and to Hugo and Lena Rabe, who provided the author.

This work was supported by the Division of Basic Energy Sciences, United States Department of Energy under contract No. W-7405-ENG-48 through the Materials and Molecular Research Division of Lawrence Berkeley Laboratory.

REFERENCES

1. D. H. Jack and J. Nutting: Intl. Met. Reviews, 1974, 19, p. 90.

2. G. Thomas: Met. Trans., 1971, 2, p. 2373.

3. C. M. Wayman: Metallography, 1975, 8, p. 105.

4. J. McMahon and G. Thomas: Proc. Third Intl. Conference on Strength of Metals and Alloys, Inst. of Metals, London, 1973, 1, p. 180.

5. R. Clark and G. Thomas: Met. Trans., 1975, 6A, p. 969.

6. D. Huang and G. Thomas: Met. Trans., 1971, 2, p. 1587.

7. M. Raghavan and G. Thomas: Met. Trans., 1971, 2, p. 3433.

8. G. Thomas: Battelle Colloquium on Fundamental Aspects of Structural Alloy Design, R. I. Jaffee and B. A. Wilcox (eds.), Plenum Publishing Co., 1977.

9. B. V. Narasimha Rao: Ph.D. Thesis, University of California, Berkeley, February 1978, LBL Report No. 7361.

10. B. V. Narasimha Rao and G. Thomas: to be published in Met. Trans., September 1978, LBL Report No. 8064.

11. B. V. Narasimha Rao and G. Thomas: Mat. Sci. and Engin., 1975, 20, p. 195.

12. B. V. Narasimha Rao, R. W. Miller and G. Thomas: Proc. 16th Intl. Heat Treatment Conf., The Metals Society, London, 1976, p. 75.

13. B. V. Narasimha Rao, J. Y. Koo and G. Thomas: EMSA Proceedings, 1975, p. 30, Claitors Publishind Div., Baton Rouge.

14. G. Kohn: Ph.D. Thesis, University of California, Berkeley, November 1976, LBL Report No. 5466.

15. R. M. Horn: Ph.D. Thesis, University of California, Berkeley, December 1976, LBL Report No. 5787.

16. V. F. Zacky, E. R. Parker and W. E. Wood: Proc. 3rd Intl. Conf. on Strength of Metals and Alloys, Inst. of Metals, London, 1973, 1, p. 175.

17. R. B. Nicholson: Proc. "Effect of Second Phase Particles on the Mechanical Properties of Steel," Iron and Steel Inst., London, 1971, p. 1.

18. R. F. Decker: Met. Trans., 1973, 4, p. 2495.

19. T. B. Cox and J. R. Low: Met. Trans., 1974, 5, p. 1457.

20. B. V. Narasimha Rao: M.S. Thesis, Univ. of Calif., Berkeley, June 1975, LBL Report No. 3794.

21. A. H. Cottrell: Trans. AIME, 1958, 212, p. 192.

22. N. J. Petch: Phil. Mag., 1958, 3, p. 1089.

23. G. Clark, R. O. Ritchie and J. F. Knott: Nature Phys. Sci., (London), 1972, 239, p. 104.

24. Standard Method of test for "Plane Strain Fracture Toughness of Metallic Materials," designation E 399-72, Annual ASTM standards, 1973, p. 960.

25. F. B. Pickering: Symposium: Transformation and Hardenability in Steels Climax Moly, Ann Arbor, 1967), p. 109.

26. S. K. Das and G. Thomas: Trans. ASM, 1969, 62, p. 1587.

27. G. Thomas: Iron and Steel Intl., 1973, 46, p. 451.

28. G. R. Speich and W. C. Leslie: Met. Trans., 1972, 3, p. 1043.

29. G. S. Ansell, S. J. Donachie and R. W. Messler, Jr.: Met. Trans., 1971, 2, p. 2443.

30. M. Carlson, B. V. Narasimha Rao, and G. Thomas: Met. Trans., 1979, (in press), LBL Report No. 8462.

31. E. Ness and G. Thomas: Met. Trans., 1976, 7A, p. 967.

32. Robert E. Reed-Hill: Physical Metallurgy Principles (D. Van Nostrand Company, New York, 1973), p. 716.

TABLE I.

ALLOY COMPOSITION AND TRANSFORMATION TEMPERATURES

Composition (wt%)				Measured Temp. (^{o}C)			
C	Cr	Mn	Fe	M_s	M_f	A_s	A_f
0.25	4.0	1.93	Bal.	253	164	655	685

TABLE II.

VARIATION OF MARTENSITE SIZE PARAMETERS WITH AUSTENITIZING TREATMENT IN Fe/4Cr/0.3C/2Mn ALLOY

Austenitizing Temperature (^{o}C)	Prior austenite grain size, m	Martensite packet size, m	Martensite lath width, m
900	62	29	0.38
1050	236	38	----
1100	274	40	0.39

TABLE III.

MECHANICAL PROPERTIES OF AIR-COOLED Fe/4Cr/0.3C/2Mn ALLOY

Austenitizing Temperature (°C)	Tempering Temperature (°C)	YS (KSI)	UTS (KSI)	% Reduction in Area	% Elongation Total (Uniform)	K_{IC} (KSI-in.$^{1/2}$)	Charpy V-Notch Energy (ft-lbs)
1100	as-cooled	186	231	17.9	6.6 (3.6)	69.2	11.9
	200	180	229	23.3	8.0 (4.3)	74.6	14.3
1050	as-cooled	183	230	32.1	9.3 (3.9)	----	11.9
	200	184	230	34.4	8.8 (3.6)	----	14.0
900	as-cooled	174	231	38.7	10.7 (4.1)	65.4	19.1
	200	177	230	41.2	11.8 (4.5)	77.5	19.7

TABLE IV.

X-RAY VOLUME FRACTION MEASUREMENTS OF RETAINED AUSTENITE

Austenitization Temperature (°C)	Volume Per Cent as-cooled	Volume Per Cent cooled and quenched in LN
900	5.6	2.6
1100	7.3	6.2

FIGURE CAPTIONS

Fig. 1. Cooling curves produced by monitoring the temperature of a K_{IC} test blank during air-cooling after austenitization.

Fig. 2. Sketches of round tensile (A), impact toughness (B), and plane strain fracture toughness (C) specimens (ASTM Specifications).

Fig. 3. Optical micrographs of as-cooled and cooled and tempered specimens: (a) and (b) represent the 900°C case, tempered in (b), (c) and (d) represent the 1050°C case, tempered in (d), and (e) and (f) represent the 1100°C case, tempered in (f). All heat treatments were performed for one hour and tempering was at 200°C.

Fig. 4. Schematic showing desired duplex microstructure consisting of major phase martensite contributing to strength and minor phase retained austenite providing improved toughness.

Fig. 5. Bright field micrograph showing an essentially dislocated autotempered martensite or lower bainite microstructure for the 1100°C heat treatment. Several undissolved spherical carbides are also visible, along with a small area of subsructural twinning (arrow).

Fig. 6. (a), (b) and (c): BF, DF and SAD, respectively, revealing retained austenite in the 1100°C heat treatment. The DF image is obtained using the (002) reflection of the 110 zone. The SAD pattern is analyzed in (d) and the N-W orientation relation is present.

Fig. 7. Bright-field (a), dark field (b), selected area diffraction (c) and corresponding indexed pattern (d) revealing typical widmanstatten platelets in the 1100°C treatment.

Fig. 8. Bright-field (a) of 1100°C treated sample revealing lower bainitic structure as evidenced by the orientation of carbides at 55° to the lath boundaries. Dark-field (b) revealing retained austenite at bainite lath boundareis.

Fig. 9. (a), (b), (c) and (d): Bright-field, dark field, SAD and corresponding indexed pattern, respectively, revealing retained austenite in the 900°C treated sample. Adjacent laths are found to have alternate K-S and N-W orientations. The DF image is obtained using the (002) reflection of the 100 zone.

Fig. 10. (a) BF, (b) DF, (c) SAD and (d) corresponding indexed diffraction pattern revealing widmanstatten platelets in the 900°C treatment martensite laths.

Fig. 11. Fractographs from impact toughness tests: (a) is from 900°C as cooled, (b) is from 900°C cooled and tempered at 200°C, (c) is from 1100°C as cooled, and (d) is from 1100°C cooled and tempered at 200°C.

Fig. 12. Inclusion identification for CVN fracture surfaces. (a) Fractograph and (c) corresponding EDAX analysis of large inclusion (arrowed in (a)) in the 900°C treatment and (b) fractograph and (d) EDAX analysis of inclusion (arrowed in (b)) from 1100°C treatment.

Fig. 13. Fractographs from plane strain toughness tests: (a) and (b) from the 900°C treatment in the as cooled and cooled and tempered at 200°C condition, respectively and (c) and (d) from 1100°C treatment in the as-cooled and cooled and tempered at 200°C condition respectively.

Fig. 14. Inclusion identification for plane strain toughness tests: (a) Fractograph and (c) corresponding EDAX analysis of inclusion arrowed in (a) for the 900°C treatment and (b) fractograph and (d) EDAX analysis of inclusion arrowed in (b) for the 1100°C treatment.

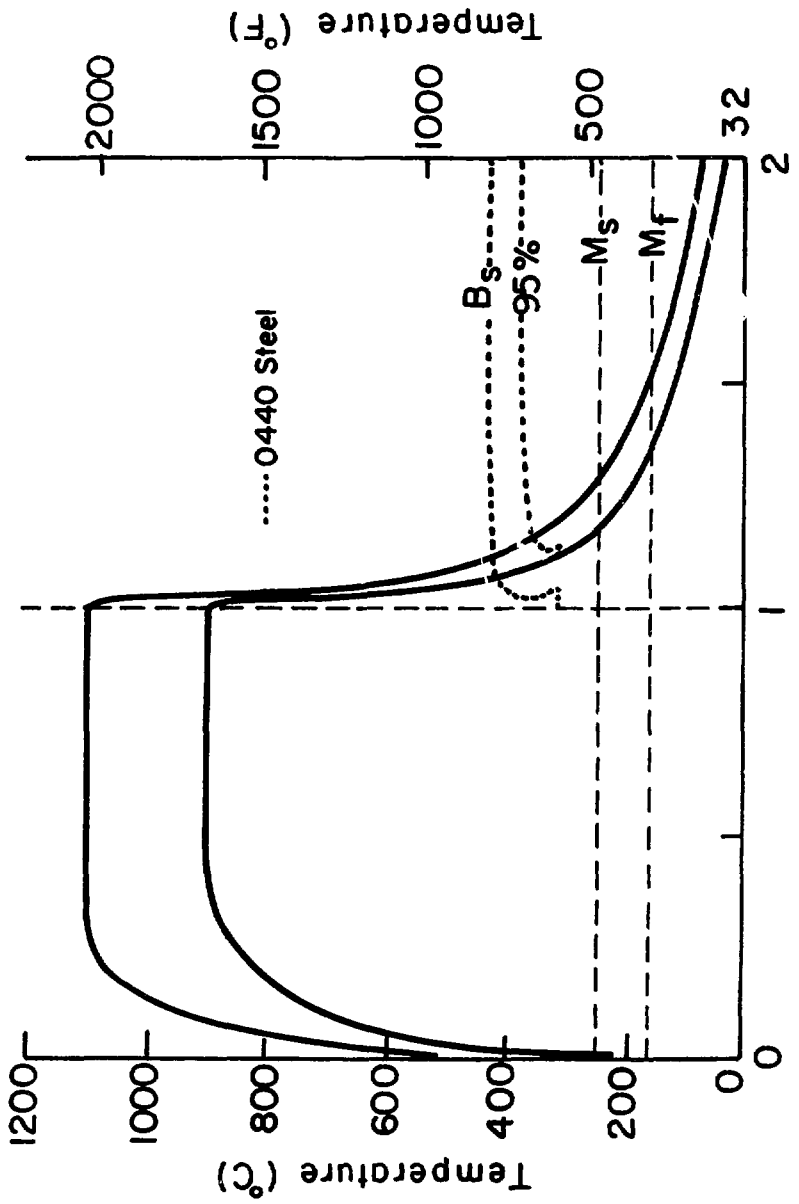

XBL 794-6200

Figure 1.

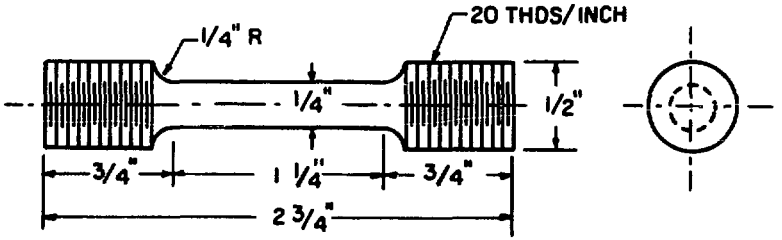

A. ROUND TENSILE SPECIMEN

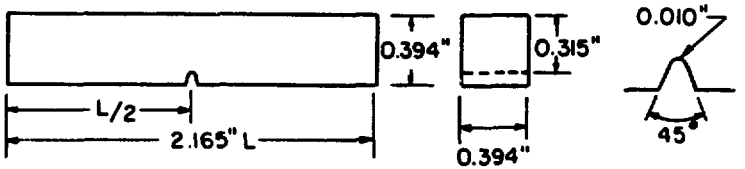

B. CHARPY V-NOTCH IMPACT SPECIMEN

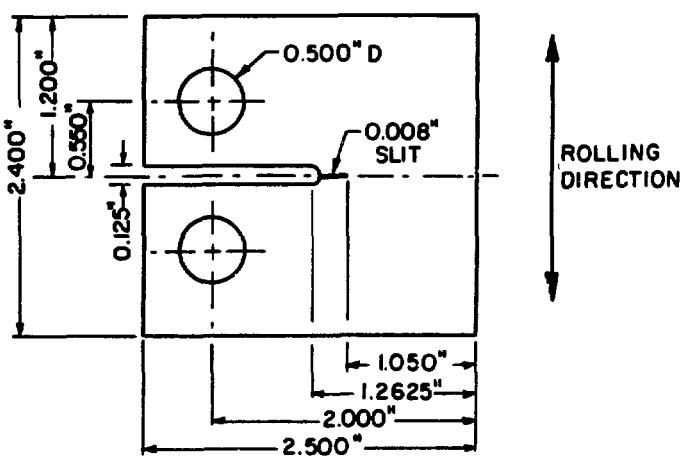

C. FRACTURE TOUGHNESS SPECIMEN

XBL 754-6176

Figure 2

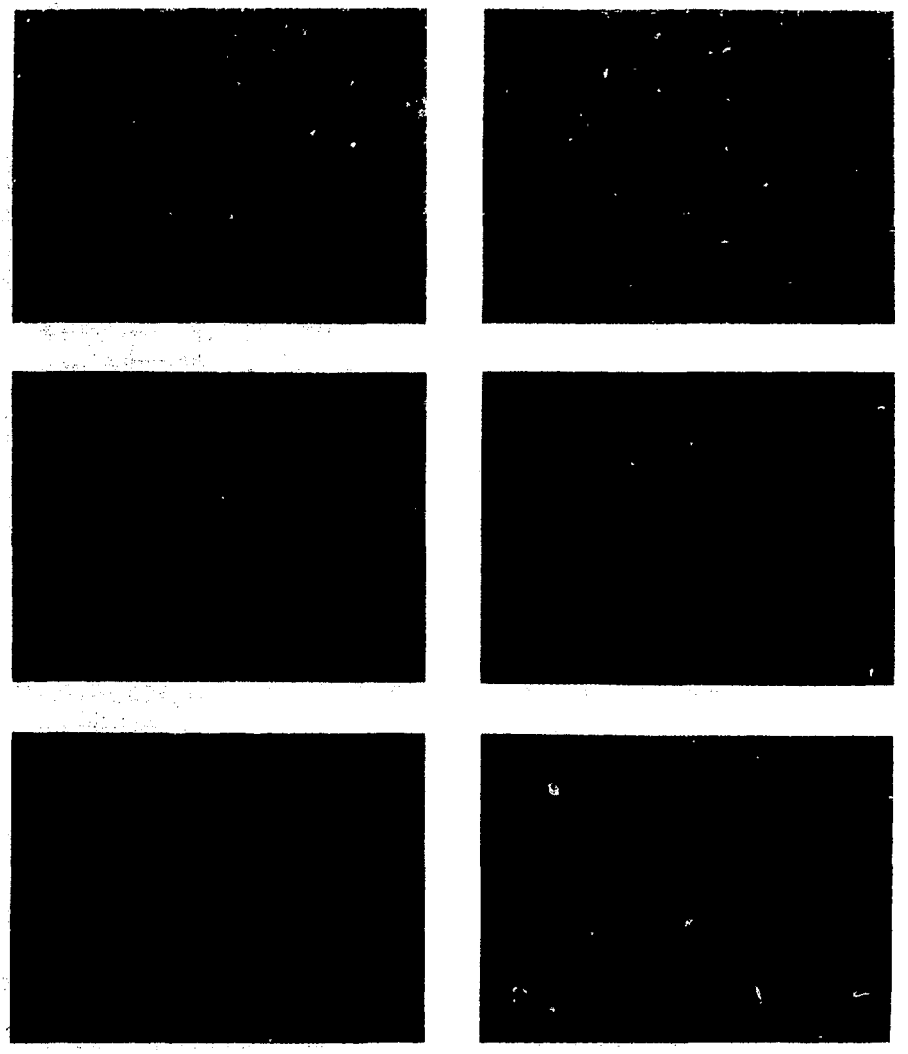

XBB794 5136

Figure 3

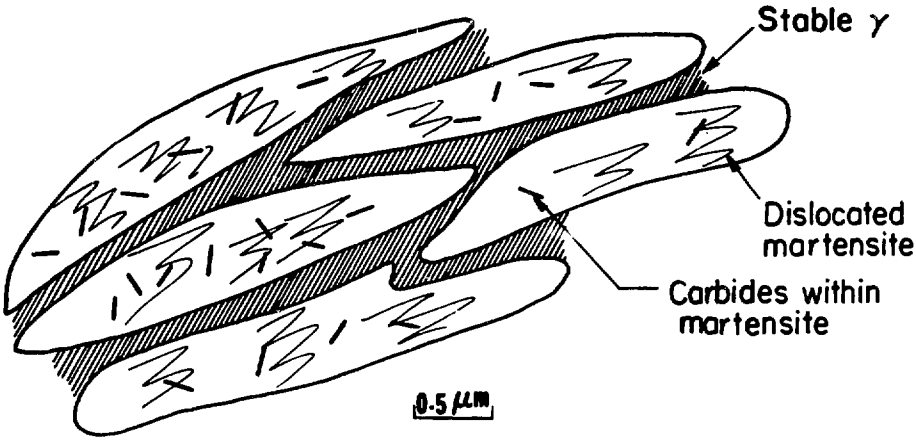

XBL 7711-10457

Figure 4

Figure 5

XBB 795-6578

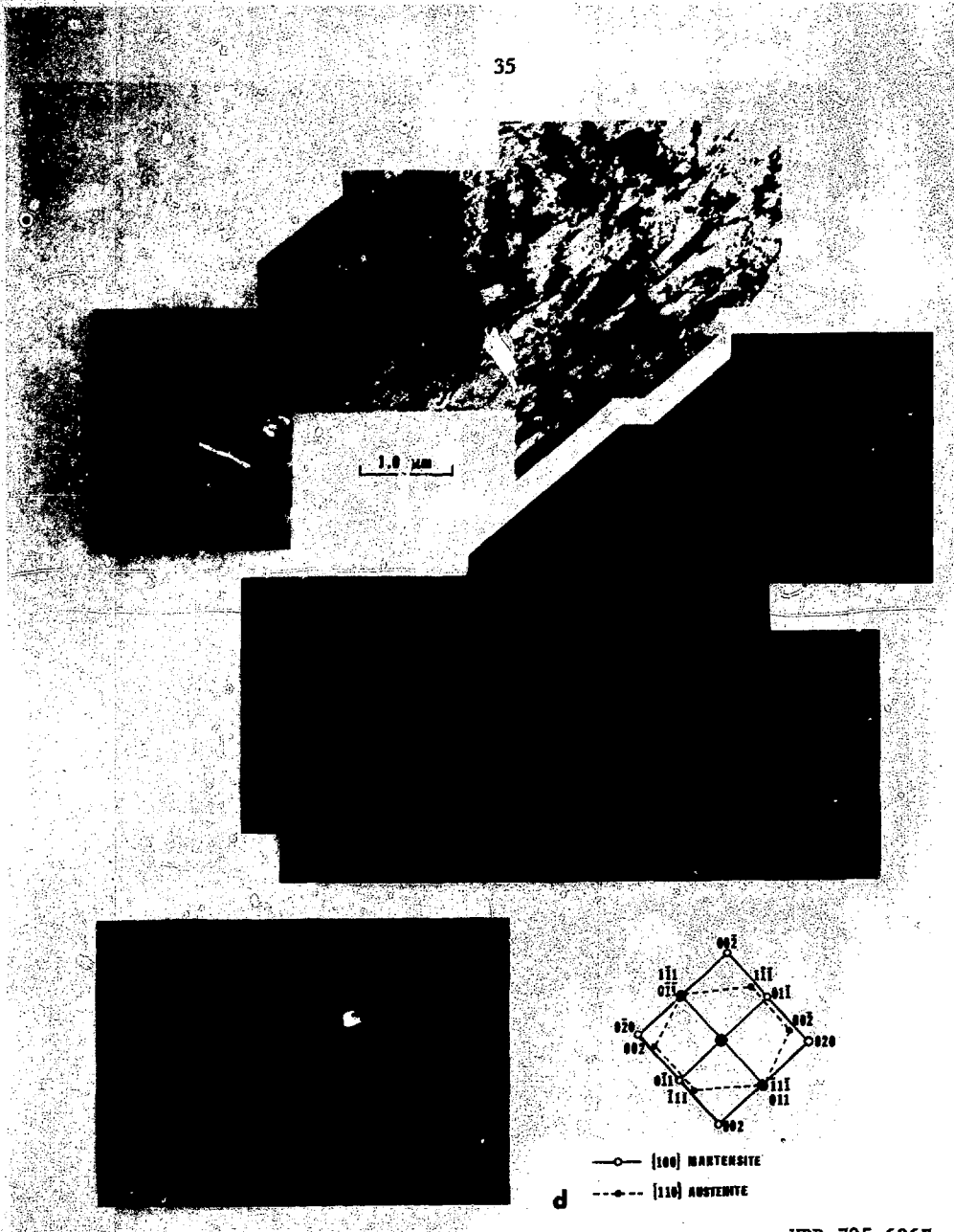

Figure 6

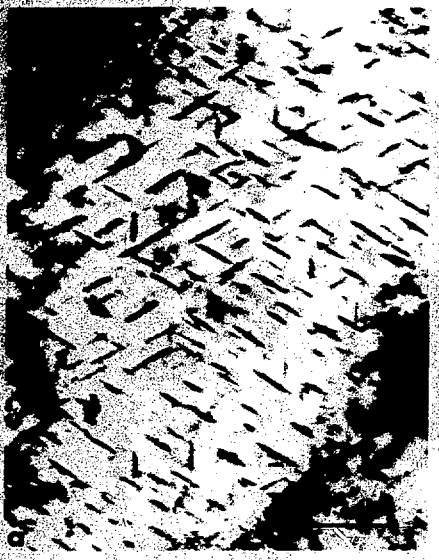

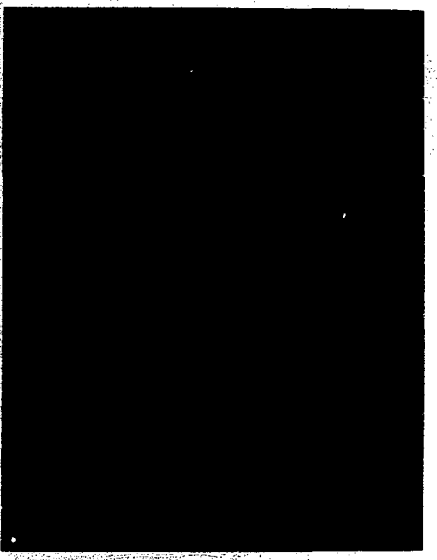

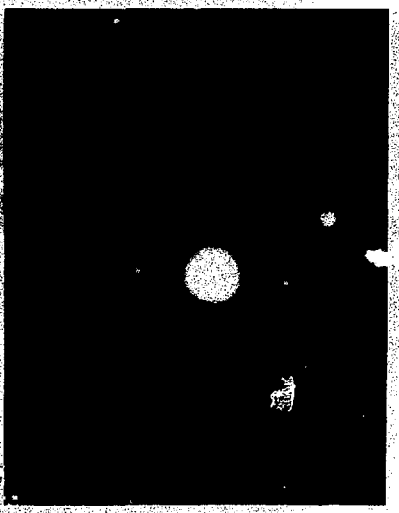

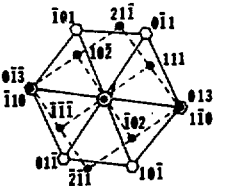

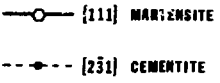

d

XBB 795-6582

Figure 7

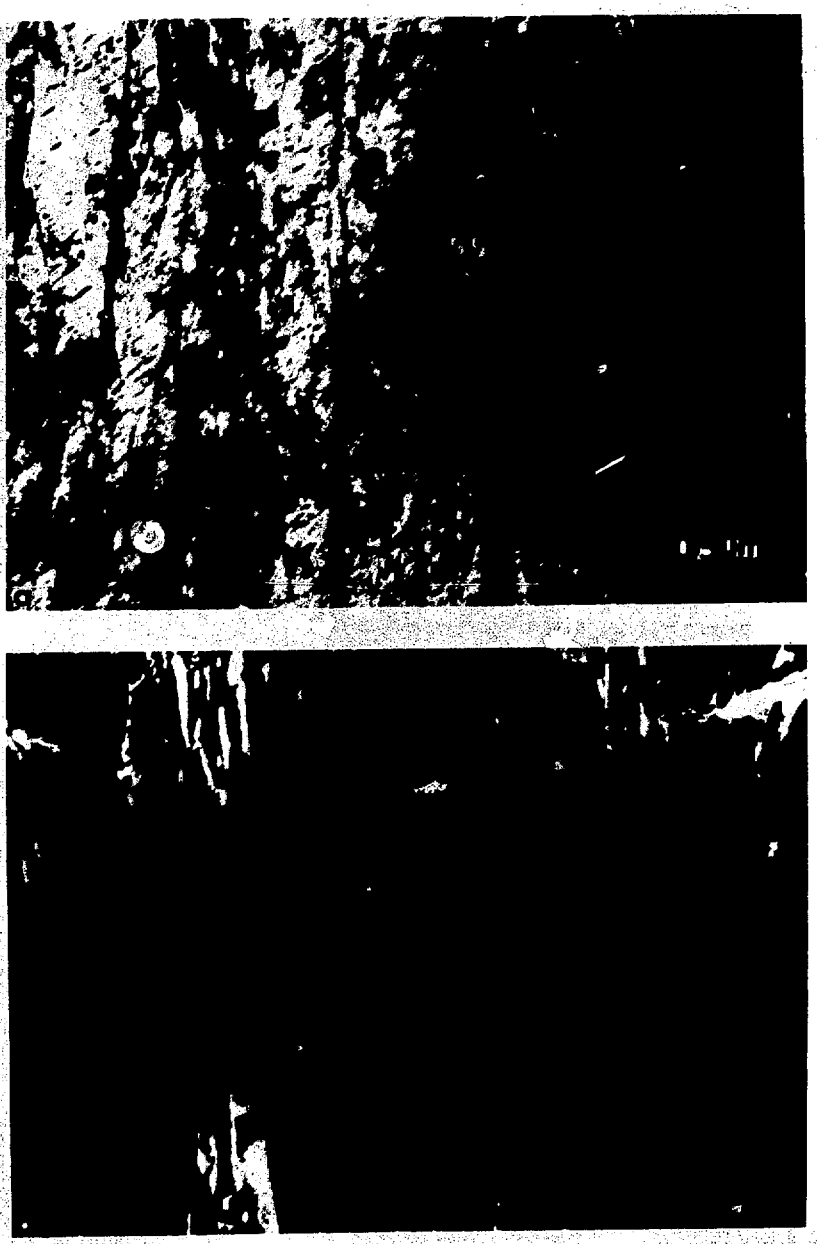

XBB 795-6581

Figure 8

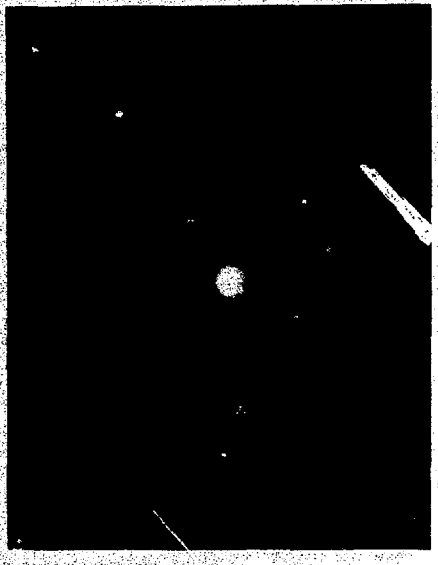

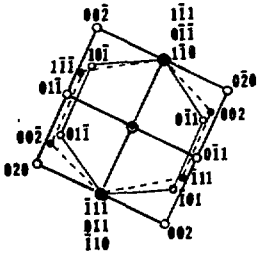

d

XBB 795-6268

Figure 9

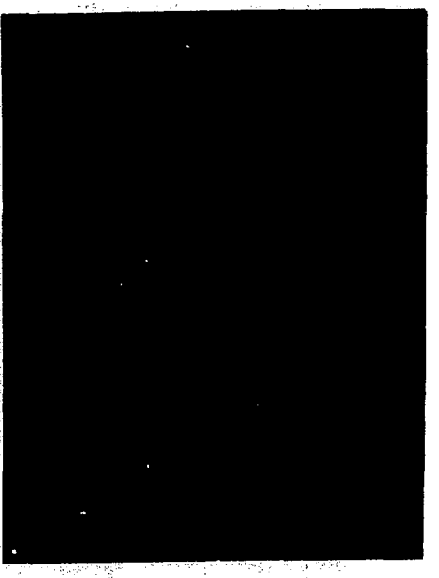

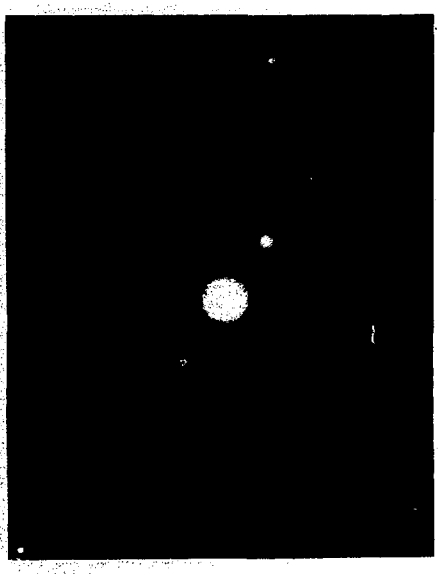

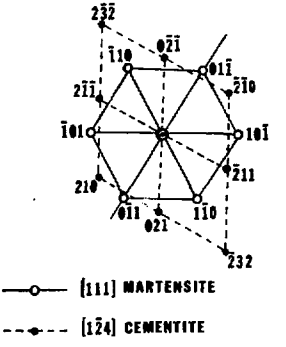

a

d

XBB 795-6269

Figure 10

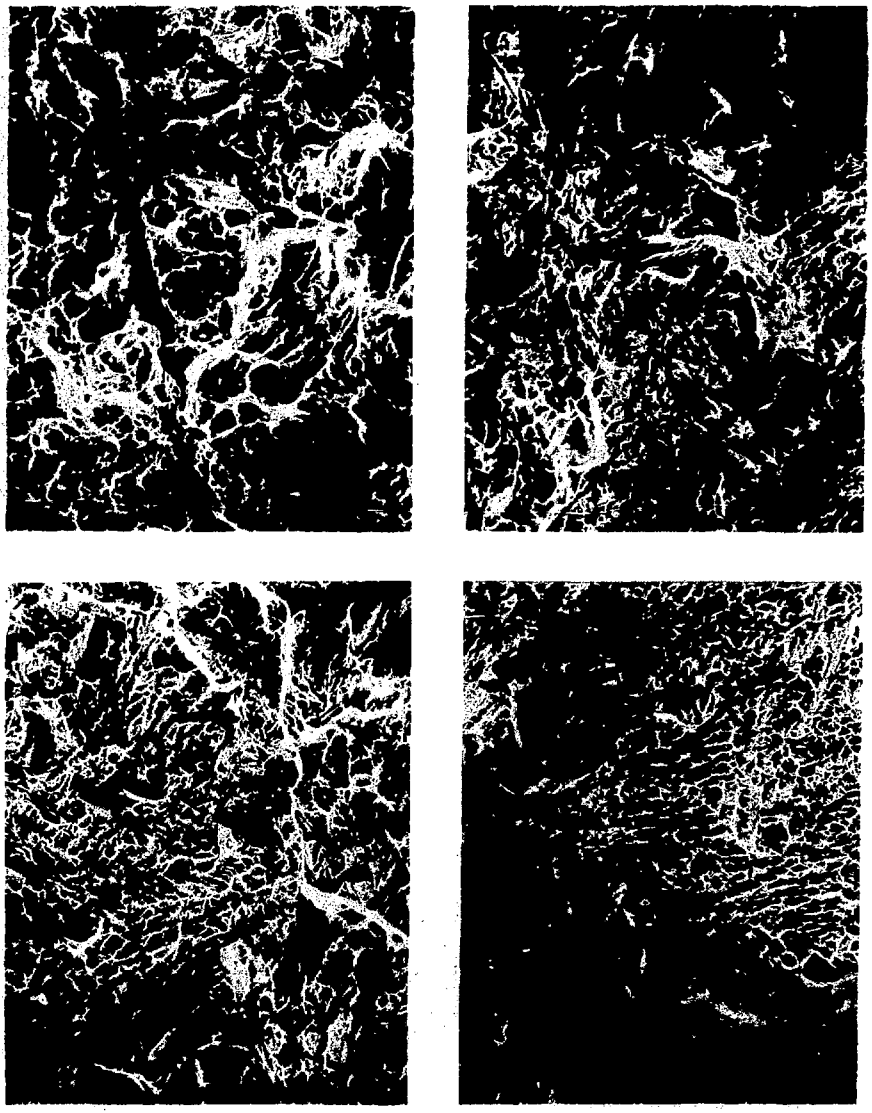

XBB 794-5139

Figure 11

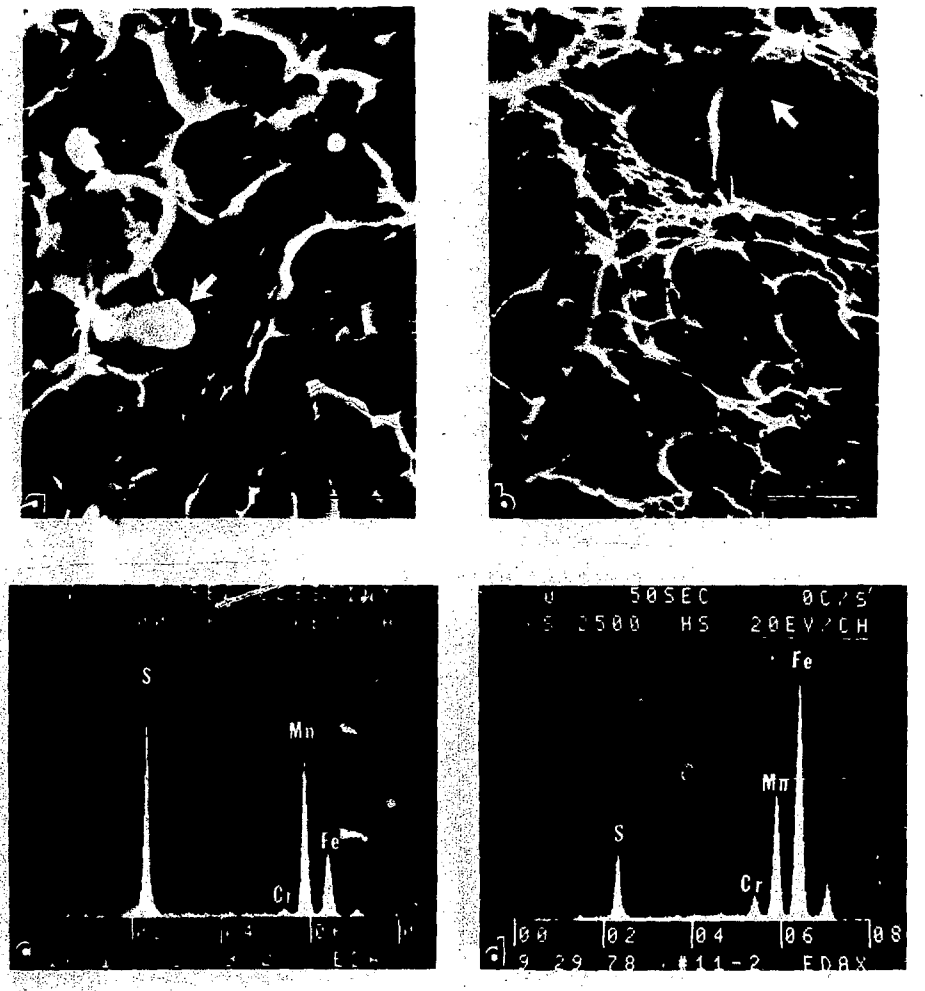

XBB 792-1656

Figure 12

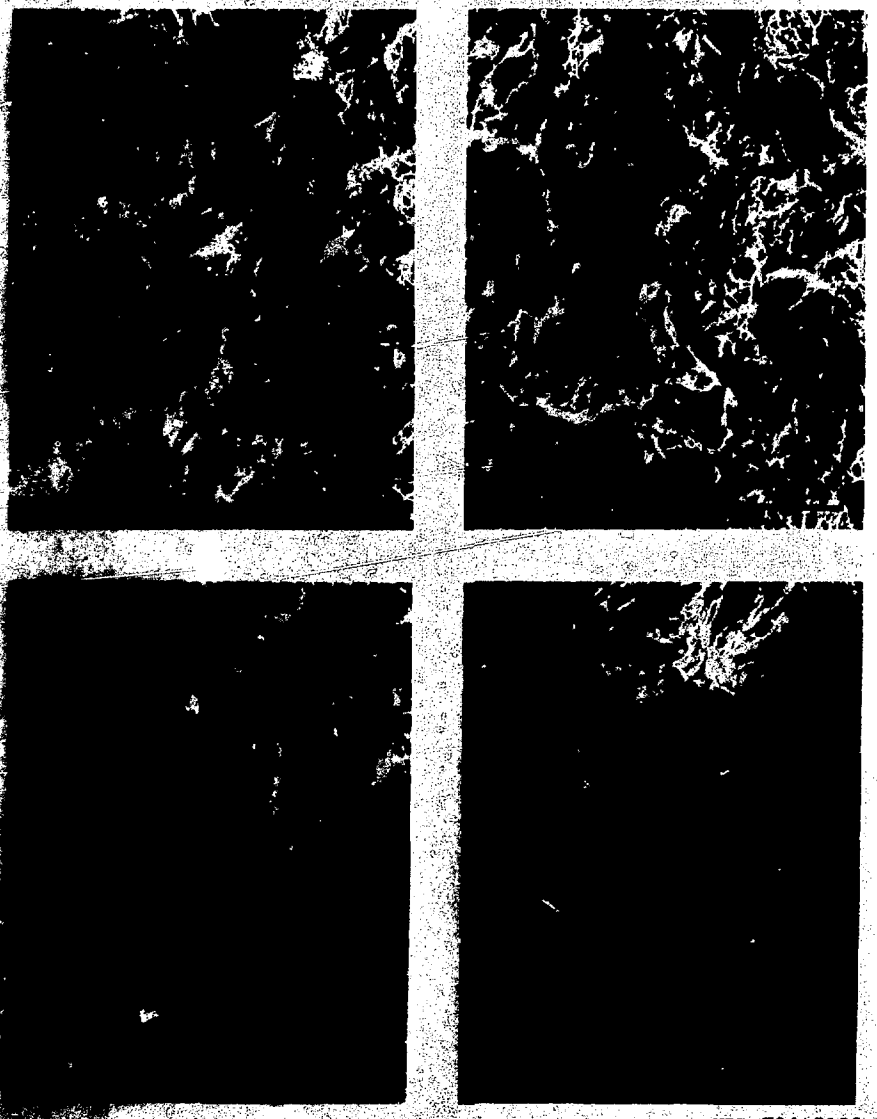

XBB 794-5138

Figure 13

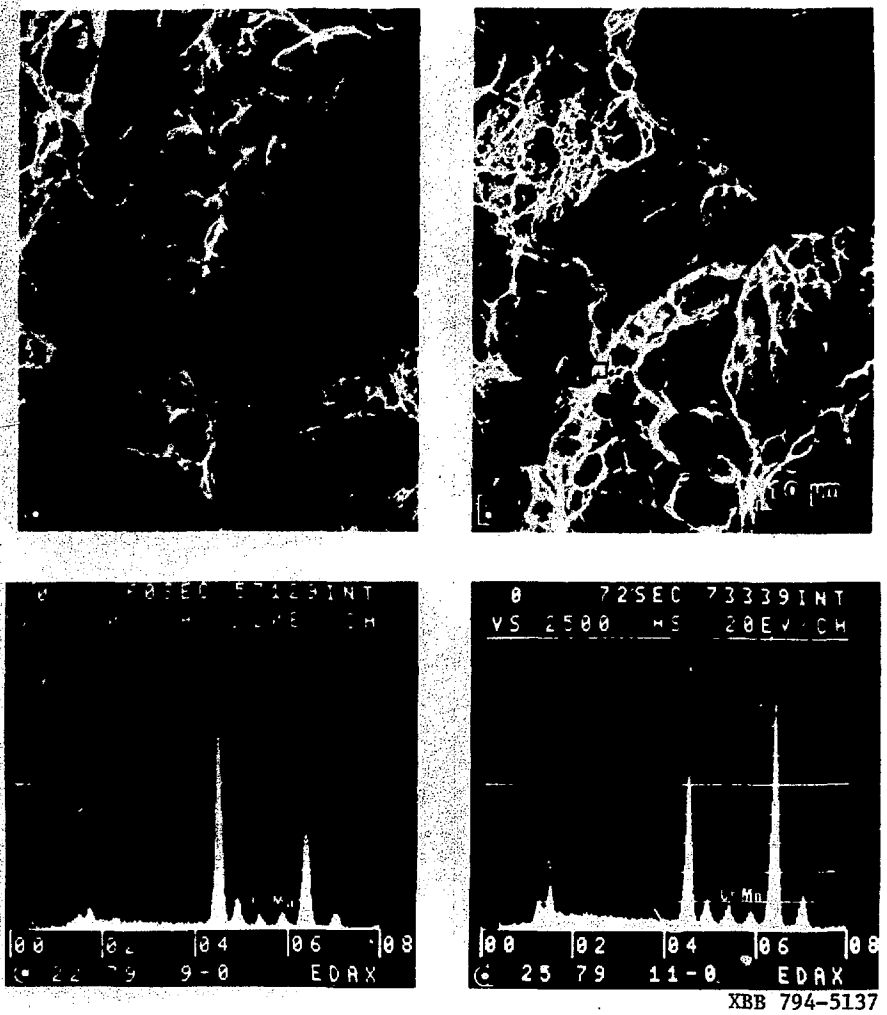

XBB 794-5137

Figure 14